Physicochemical and Microstructural Characterizations of Alkali-Activated Binder Systems

Arkamitra Kar
Department of Civil Engineering, BITS-Pilani, Hyderabad Campus, Hyderabad – 500078, India
Email: arkamitra.kar@hyderabad.bits-pilani.ac.in

Indrajit Ray
Department of Civil and Environmental Engineering, Faculty of Engineering, The University of the West Indies, St Augustine, Trinidad and Tobago
Email: Indrajit.Ray@stu.uwi.edu

Udaya B. Halabe
Department of Civil and Environmental Engineering, West Virginia University, Morgantown, WV 26506, USA
Email: Udaya.Halabe@mail.wvu.edu

Avinash Unnikrishnan
Department of Civil and Environmental Engineering, Portland State University, Portland, OR, USA 97201 USA
Email: avinashu@gmail.com

***Abstract*—Alkali-Activated Binder (AAB) is being considered as a sustainable and greener alternative to portland cement binder due to their low carbon dioxide footprint and effective byproducts/waste better recycling capacity. For better understanding of AAB behavior the present study has conducted a number of physicochemical and microstructural characterizations of ten different combinations of AAB containing fly ash and/or slag at three different curing conditions. Results revealed the presence of Si-O-Si bonds, Si-O-Al bonds, and sodium aluminosilicate for pure fly ash based AAB. Ca^{2+} ions and calcium silicate hydrate were present under the influence of slag. This information will help in estimation of volume fractions of different AAB mixtures from microanalysis data.**

***Index Terms*—alkali-activated binder, degree of reaction, FTIR, isothermal calorimetry, SEM/EDS, XRD**

I. Introduction

Portland cement concrete industry contributes at least 5–8% of the global carbon dioxide emissions [1]. Besides greenhouse gas, the production of cement is energy intensive and causes depletion of natural limestone resources. The recent proliferation of construction in emerging countries significantly increased the consumption of portland cement. To overcome this problem, there is a strong need is to develop an alternative binder which would be greener and more sustainable than portland cement. One such promising material is Alkali Activated Binder (AAB) or inorganic polymer binder. In 1981, Professor Davidovits of France produced a new type of binder by mixing alkalis with burnt mixture of kaolinite, limestone and dolomite [2]. The binders were known as "geopolymer" since they were originated by inorganic polycondensation, or "geo-polymerization" [2], [3] of primarily aluminosilicate compounds. This is also popularly known as Alkali-Activated Binder (AAB) because these binders can be produced by alkali-activation of aluminosilicates mixed with other ions like calcium ions. Early researches have shown that AAB are relatively less expensive to produce when some commonly available naturally occurring materials are mixed with NaOH and water [4]. Another major incentive for development of such binders is the fact that the annual output of fly ashes from power plants and other byproducts are so enormous that there is a constant need to find new uses for them. In the US, approximately 49% of the utility wastes are simply landfilled, 41% are contained in surface impoundments, and about 10% are disposed of by discharging into old quarry operations [1]. During the past two decades, AAB concrete have attracted strong interests all over the world because of their much lower emissions of carbon dioxide, lower energy cost, and better recycling capacities of wastes and byproducts compared to portland cement concrete [4]-[6].

In order to encourage widespread use of this new binder a detailed investigation is needed to clearly understand the physicochemical and microstructural properties of AAB among other properties. This

Manuscript received September 11, 2015; revised January 8, 2016.

doi: 10.18178/ijscer.5.2.119-129

information will provide insights into the long-term performance of AAB. Although previous research reported the successful use of various wastes and byproducts to produce AAB, their curing effects, and strength and durability characteristics over time [2], [4], [6], [7], limited information is available on the physicochemical and microstructural characteristics which explains the chemical and physical reactions those take place behind the formation of AAB products. Literature review shows that analytical techniques such as X-ray Diffraction (XRD) [8]–[12], Fourier Transform Infrared (FTIR) spectroscopy [13]–[16], Scanning Electron Microscopy and Energy Dispersive X-Rays (SEM-EDS), and thermal analysis have been used to characterize the alkali-activation of different precursors [17]–[21]. In most of the cases, the aluminosilicate precursor was used without the inclusions of other ions to ensure pure geopolymeric type of reactions [8]-[10], [13], [16], [19], [21]. In few cases the combinations of ions from byproducts such as Class C and Class F fly ash, metallurgical slags, and calcined clay were used [4], [11]. However, in these cases limited characterization techniques were used.

A significant step towards the successful implementation of AAB will be to accurately estimate the volume fractions of AAB produced from different sources of fly ash and slag through microanalysis and stoichiometry of the reaction products. In order to accomplish this, it is essential to characterize the AAB at microlevel using different techniques and identify the relevant chemistry of polymerization and reaction products. To address this problem, the current research will (1) obtain the optimum ratios of precursor and activating solution to find the best AAB through their compressive strengths; (2) identify the chemistry of polymerization and the dominating chemical bonds due to the interaction between alkali activated fly ash and/or slag; (3) identify the degree of reaction ; and (4) form the basis of estimation of volume fractions of different AAB mixtures from microanalysis and volume stoichiometry.

The microanalysis techniques adopted for the present study are X-Ray Diffraction (XRD), Fourier Transform Infrared (FTIR) Spectroscopy, Scanning Electron Microscopy (SEM), Energy Dispersive X-Ray Spectroscopy (EDS), Degree of reaction, and Isothermal calorimetry. A total of ten AAB binder systems were studied. The XRD study was conducted to confirm the amorphous state and identify the presence of minerals. The FTIR was conducted to identify the Si-O-Si as well as Si-O-Al bonds and the presence of unreacted raw materials. The SEM/EDS was aimed to observe the reaction products and progress of the reactions for different AABs, and to identify the various phases formed due to variations in the precursor and temperature of curing. The degrees of reaction were studied to corroborate the findings of the reaction rates as observed by other methods. The isothermal calorimetry study was used to confirm the degree of reaction due to temperature changes.

II. Materials and Mixture Selections

A. Materials

Class F fly ash used in this study conforming to [22], was obtained from a local coal power plant. The specific gravity, specific surface area and oxide composition are listed in Table I. Ground granulated blast furnace slag or slag conforming to Grade 100 of [23] obtained from local steel plant was used in this study (Table I).

TABLE I. Properties of the Materials Used

MATERIALS	SLAG*	FLY ASH
Specific gravity	2.88	2.47
Specific surface (m^2/kg)	580 (Blaine)	490 (Blaine)
Loss on ignition (%)	0.06	3.00
SiO_2, %	36.0	49.34
Al_2O_3, %	12.0	22.73
CaO, %	42.0	3.0
MgO, %	6.0	1.06
SO_3, %	0.2	0.97
$Na_2O + 0.685\ K_2O$, %	0.74	2.75
Fe_2O_3, %	1.8	16.01
Others, %	1.2	1.05

*The pH value (in water) for the slag is in the range of 10.5 ~ 12.7.

The coarse aggregate used was 12.5 mm graded and crushed limestone conforming to [24]. The Saturated Surface Dry (SSD) bulk specificgravity was 2.68. Locally available 4.75 mm graded river sand conforming to [24] was used in this study. The fineness modulus and the SSD bulk specific gravity of sand are 2.79 and 2.59, respectively. A commercially available High-Range Water Reducing Admixture (HRWRA), conforming to [25] was used in this study.

TABLE II. Preliminary Scheme for Selection of Precursor Combinations

Precursor	**Alkali activating solution, AAS ($Na_2O.2SiO_2$ + NaOH)**	**Curing temps**	**Age (days)**
100 % Fly ash	Total SiO_2 / Na_2O = 1.2, 1.4, 1.6, 1.8	23 ℃, 40 ℃, 60 ℃	3, 7, 28

B. Mixture Proportions Selections

Initially in order to estimate the best Ms (SiO_2/Na_2O) modulus ratio, the compressive strengths of 50 mm AAB cube specimens were determined with 100% fly ash as precursor and different alkali-activating solutions for Ms =1.2, 1.4, 1.6, and 1.8, respectively at three different curing temperatures. The quantity of coarse aggregate was kept constant at 1209 kg/m^3 and that of fine aggregate at 651 kg/m^3 for all concrete mixtures. These preliminary schemes of mixtures are shown in Table II. The compressive strength values are shown in Figs. 1(a) through 1(c). From the figures, it is evident that Ms of 1.4 resulted in the best compressive strengths at all ages and the strengths consistently increased with the increase in curing temperature.

TABLE III. FINAL CONCRETE MIXTURE PROPORTIONS FOR ALKALI ACTIVATED FLY ASH AND/OR SLAG (MS MODULUS = 1.4).

Precursors	Mixtures	Fly ash	Slag
		Kg/m^3	Kg/m^3
100 % Fly ash	FA 100	400	0
85% Fly ash + 15% slag	FA 85 SG 15	340	60
70% Fly ash + 30% slag	FA 70 SG 30	280	120
50% Fly ash + 50% slag	FA 50 SG 50	200	200
30% Fly ash + 70% slag	FA 30 SG 70	120	280
15% Fly ash + 85% slag	FA 15 SG 85	60	340
100% slag	SG 100	0	400
Pre blend 100% fly ash and solid NaOH for 15 days	FA 100 p15	400	0
Pre blend 100% fly ash and solid NaOH for 30 days	FA 100 p30	400	0
Pre blend 100% fly ash and solid NaOH for 60 days	FA 100 p60	400	0

Note: Quantity of Sodium silicate (liquid) was 129.43 kg/m^3 and that of sodium hydroxide (solid) was 10.57 kg/m^3 for all mixtures. The quantity of coarse aggregate was kept constant at 1209 kg/m^3 and that of fine aggregate at 651 kg/m^3 for all mixes. The quantity of HRWRA used was in the range of 5060 ~ 6745 ml/m^3.

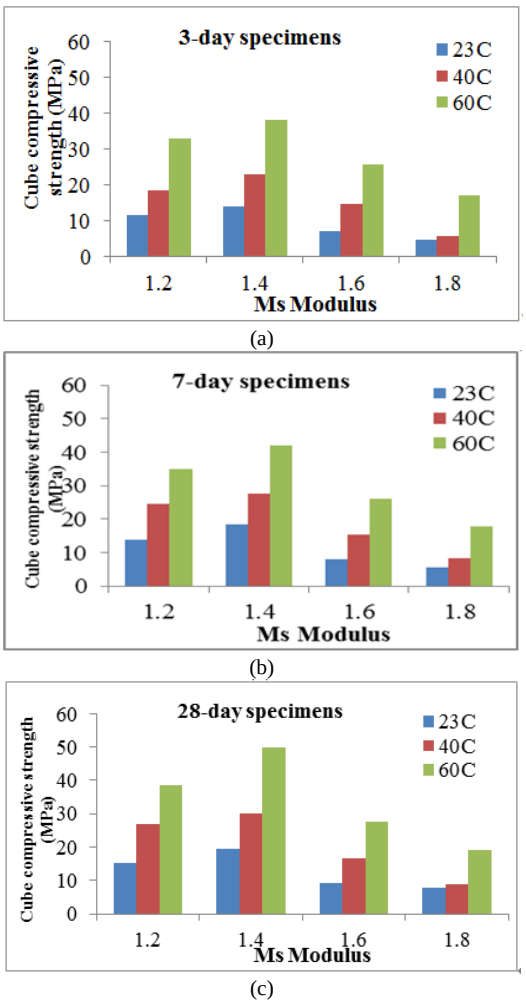

Figure 1. Cube compressive strength for mixtures from Table II at different Ms Modulus for specimens at different ages: (a) 3 days, (b) 7 days, and (c) 28 days.

Based on this optimum value of Ms the mixture proportions for AAB pastes were selected by combining different percentages of fly ash and slag for physicochemical and microstructural tests. Additionally few cases of preblended fly ash and NaOH were also included in the study to observe the effects of preblending of alkaline agents on the precursor and the subsequent polymerizations. Three different exposure days (15, 30, and 60, respectively) of preblending were maintained. No coarse aggregates and fine aggregates were added in these mixtures. The selection of mixtures was done to be able to compare only fly ash, different combinations of fly ash + slag, and only slag as precursors at different ages and curing temperatures. A total of ten mixtures were produced at each of the three different temperatures: 23˚C, 40˚C, and 60˚C.

III. EXPERIMENTAL PROGRAM

A. X-Ray Diffraction(XRD)

X-ray diffraction was performed on all samples using a Bruker D8 Discovery X-ray Diffractometer. The CuKα X-rays were generated at 40 mA and 40 kV. Scans were performed over 5 to 70° 2θ range at 0.02° 2θ steps and integrated at the rate of 2 seconds step^{-1}. The powder samples used for the XRD analyses were obtained by crushing the hardened samples of AAB and passing through 45 micron sieve. The chemical reactions that produce the polymer products when fly ash is activated with an alkali solution are very sensitive to the ambient conditions of temperature and relative humidity. Hence, the above arrangement was adopted to ensure that the samples used for different microanalysis techniques were all generated from the same source and the corresponding chemical reactions took place under identical ambient conditions of temperature and relative humidity.

B. Fourier Transform Infrared Spectroscopy (FTIR)

The chemical compositions and the structural bonds present in the AAB samples were investigated by Fourier Transform Infrared (FTIR) spectroscopy. FTIR spectra were obtained using a PerkinElmer Spectrum 100 FTIR spectrometer with Universal ATR accessory, in absorbance mode, within the frequency range of 4000 – 400 cm^{-1}. The powder samples for FTIR were obtained by crushing the hardened samples of AAB and passing through 45 micron sieve.

C. Scanning Electron Microscopy (SEM) and Energy Dispersive X-Ray (EDS)

A state-of-the-art thermal Field Emission Scanning Electron Microscope (FE-SEM), JSM-7600F (accompanied by an EDS analyzer), supplied by JEOL Limited was used for the imaging process. The samples were cast in small ampoules. They were extracted and then polished mechanically to make the final average thickness of about 2.5 mm. Before SEM and microanalysis by EDS, the samples were allowed to dry at 50% humidity and 40˚C for 48 hours in an environmental chamber to reduce the time of vacuum. Then they were coated with a 15 nm layer of platinum in

argon gas atmosphere at a high vacuum of 5.0 x 10^{-6} Torrs, in order to make them electrically conductive in nature. The samples were stored in 99.8% laboratory grade methanol in air-tight vial until the SEM studies were conducted to stop the continued hydration at respective ages. In order to get good resolution of the SEM/EDS the surfaces of the samples had to be polished before the microanalyses. The samples were polished using a TegraPol-31 fitted with Tegra Force 5 machine by Struers Inc. For each location, five EDS spectra were acquired with the help of the INCA systems software that is used by the Oxford spectrometer. The working distance was maintained at 15 mm and the probe current 8 (65.4 ~ 67.0 μA) in order for the EDS analyzer to work properly. Each sample was approximately divided in three locations. The microanalysis was done at five randomly chosen points for each location at each magnification for every sample. Thus for each sample, for three locations, at each magnification, 45 points were analyzed. Finally for two magnifications (2500x and 5000x), 90 points were analyzed for each of the ten different mixtures at every age (7, 28, and 90 days). The points for microanalysis were chosen randomly to minimize the influence of the heterogeneity of the AAB microstructure. In selected locations of sample, also average microanalysis (not point analysis) was conducted to verify the variations compared to point analysis. Out of the 90 points, 60 points were used to formulate the model used for estimating the volume of the hydrated products and the remaining 30 points were used to validate the predictions from the proposed model. These 60 points were chosen randomly for the same reason as mentioned above. As typical examples for a given mixture proportion and 2500x magnification, Figs. 7 (a) and (b) show EDS images for FA 100 AAB and FA 50 SG 50 AAB with curing temperature of 40˚C. A similar procedure was followed for the other cases. The matured AAB were observed under the SEM at two different magnifications – 2500x and 5000x.

D. Degree of Reaction at Different Ages

As mentioned earlier, the samples were cured at three different temperatures. One of the major factors that govern the progress of polymerization, is the curing temperature. Therefore, it is of utmost importance to have knowledge of the influence of the curing temperature on the degree of reaction. The technique suggested by [26], [27] was followed here to determine the degree of reaction. After curing (at each respective temperature), the alkali activated fly ash was reacted with 1:20 HCl to determine the amount of fly ash that had been converted to sodium aluminosilicate phase and the portion that remained unreacted with the alkaline solutions. The experimental procedure followed in the acid attack consisted in adding 1 g of activated fly ash to a beaker containing 250 ml of (1:20) HCl. The mixture was stirred with a plastic rotor for three hours, after which it was filtered and washed with de-ionized water to a neutral pH. The insoluble residue was first dried at 100˚C and then at 1000˚C. The 1000˚C was attained using an Isotemp Muffle Furnace from Fisher Scientific. The degree of reaction, α_{FA}, was found by determining weight loss with respect to their original weights expressed in fraction.

E. Isothermal Calorimetry

The calorimetry test was conducted to evaluate the rate of hydration of AAB samples per [28]. The calorimeter used was the TAM-Air model manufactured by TA Instruments. The sealed ampoule arrangement was followed and the data were collected using the TAM Assistant software built-in with the machine. The experiments were carried out on 5 grams of AAB sample for each mixture at temperatures of 23˚C, 40˚C, and 60˚C (with a variation of ±0.2˚C in each case).

IV. Results and Discussions

A. X-Ray Diffraction (XRD)

XRD diffractogram for a 28-day AAB sample containing 100% fly ash with Ms modulus = 1.4, curing temperature of 40 ℃, and w/s = 0.20 is shown in Fig. 2. The 2-theta range for observing the XRD pattern was varied from 0 ° to 100 °. This sample showed predominantly X-ray amorphous character.

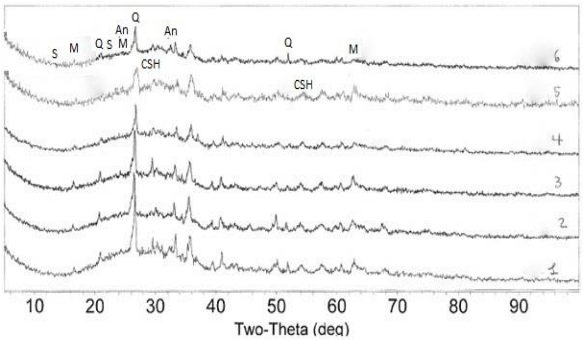

Figure 2. XRD results for six different mixture proportions and each sample being tested at 28-day age – (1) FA 100 cured at 23˚C, (2) FA 100 cured at 40˚C, (3) FA 100 cured at 60˚C, (4) FA 50 SG 50 cured at 40˚C, (v) SG 100 cured at 40˚C, and (6) FA 100 preblended with NaOH for 7 days and cured at 40˚C. (S=hydroxy sodalite, M=Mullite, Q=Quartz, An=Analcime, CSH=Calcium silicate hydrate due to slag, CSH(S)).

Peaks of quartz (SiO_2) and mullite ($Al_6Si_2O_{13}$) were visible along with those of analcime ($NaAlSi_2O_6 \cdot H_2O$) and hydroxy sodalite ($Na_6(Si_6Al_6O_{24}).8H_2O$). The respective peaks have been denoted by Q, M, An, and S, in Fig. 2. Those peaks showed the presence of sodium aluminate chemical bonds having (Si-O-Al) chemical structure. Peaks were also observed for analcime and hydroxy sodalite where the Na^+ cation has penetrated into the aluminosilicate (Si-O-Al) chemical structure. Polymerization proceeded as Na entered into the Si-O-Al structures. The hump or the shoulder in the figure also confirmed the presence of amorphous phases co-existing with crystalline phases.

XRD diffractograms obtained for unreacted fly ash powder (not shown here for brevity) were quartz (SiO_2) and mullite ($Al_6Si_2O_{13}$). The matured AAB showed the presence of quartz, mullite, analcime and hydroxy sodalite which were identified by their characteristic

peaks. The matured AAB also showed the presence of an X-ray amorphous aluminosilicate material, demonstrated by the broad hump from approximately 20 to 40º2θ. It can be seen from Fig. 4.2 that no significant change in intensity for the quartz or mullite peaks was observed in the AAB samples. This was expected, because it is predominantly the X-ray amorphous (glassy) phases in fly ash that undergo dissolution and subsequent geopolymerisation at high pH. The hump in the region of 20 ° to 40 ° 2θ is characteristic of amorphous silica. This indicated that there may be some unreacted fly ash in the system.

Another notable feature was the formation of hydroxy sodalite, a low silica zeolite ($Na_6(Si_6Al_6O_{24}).8H_2O$). The samples showed some small peaks in regions indicating minor sodalite formation. This could occur if the silica dissolved slowly and the silicate species in solution did not migrate far from the particle surface. This results in regions which are silica rich and others which are silica deficient.

It is possible that the silica deficient gel is able to form the low silica crystalline hydroxy sodalite phase, while the X-ray amorphous phase with higher silicate content binds the phase separated system. These observations were in close agreement with the findings from previous researchers [10], [11], [29].

In the case of samples containing either slag or a combination of fly ash and slag as precursor, the presence of calcium silicate hydrate due to slag hydration, CSH(S) was observed from the small peaks which represented the amorphous calcium silicate hydrate matrix. These observations were in compliance with the findings from previous researchers [30], [31]. The XRD results for sample 5 (Fig. 2), which corresponds to the case of SG 100 cured at 40˚C, showed the presence of Calcium Oxide peaks. This occurrence indicates the formation of calcium silicate hydrate [CSH(S)] in the microstructure of the polymer product as a result of slag hydration. The slag hydration process was assumed to be similar to portland cement hydration. It results in the formation of calcium silicate hydrate matrix similar to the case of portland cement but having a different Ca/Si ratio. This hydration takes place simultaneously with the polymerization reactions related to the alkali activation of fly ash.

Other than those mentioned above, no new crystalline phases were identified as products of the reactions. Although XRD is an analytical technique commonly used to investigate AAB systems, the technique has significant limitations due to the apparent amorphous nature of AAB materials. Since the present study requires knowledge about the quantity of the different phases in the microstructure of the polymer product, other analytical techniques need to be used in conjunction with XRD to provide insight into the microstructural characteristics of AAB. FTIR studies were conducted to corroborate the XRD results because of the uncertainty in the microstructural composition of the polymer product.

B. Fourier Transform Infrared Spectroscopy (FTIR)

The FTIR spectra for the matured AAB and unreacted precursor, i.e., fly ash and/or slag before alkali-activation, are shown in Fig. 3. The FTIR spectra were collected for both the precursor (fly ash powder) and the finished product (28-day age AAB sample with 100% fly ash at Ms modulus of 1.4 and w/s = 0.2). The figure compares the absorbance spectra for fly ash powder and AAB containing 100% fly ash at three different temperatures of 23˚C, 40˚C and 60˚C. The spectra for AAB containing 100% fly ash at 23˚C shows a chemical shift of about 10 cm^{-1} in the range of wave number of 1008 cm^{-1}.

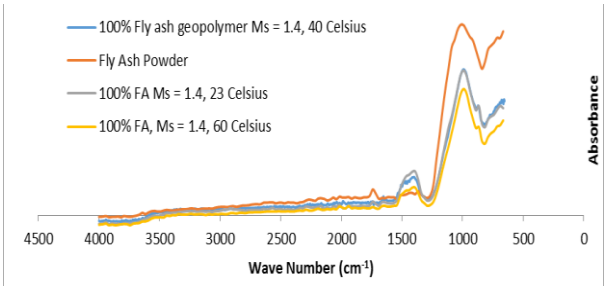

Figure 3. Comparing FTIR absorbance spectra of fly ash powder and 100% fly ash based AAB.

This shows the progress of the polymerization reactions. Also, the spectra for AAB with 100% fly ash at 60˚C show a chemical shift w.r.t. the spectra corresponding to the AAB with 100% fly ash at 40˚C. In other words, the chemical shift increases with increase in curing temperature. This was an indication of the increased rate of reaction with the increase in curing temperature. The results are consistent with the findings made by [15], [31]. Presence of Al-OH bonds were also detected in each of the AAB spectra in the region of 910 cm^{-1}. Peaks associated with amorphous silica appear at around 1000 cm^{-1}, 900 cm^{-1} and 500 cm^{-1}, these peaks correspond respectively to the stretching, bending, and rocking of the Si-O-Si bond. The peak near 1000 cm^{-1} was observed at 1043 cm^{-1} for the raw fly ash powder. This wave number was taken as the datum w.r.t. which the peak shifts for all the AAB samples were calculated.

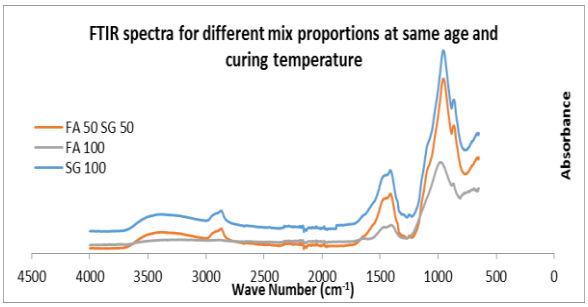

Figure 4. Comparing FTIR absorbance spectra of FA 100, FA 50, SG 50, and SG 100 AAB samples

As evident from Fig. 4, the peaks near 1000 cm^{-1} and 900 cm^{-1} are of lower intensity for all AAB samples, compared to the raw fly ash powder. This indicated that silica in raw fly ash powder has reacted to some extent to form the AAB. The FTIR spectra of all AAB samples

show a shoulder in the region of approximately 1100 cm^{-1} to 1080 cm^{-1}. This region corresponds to the strongest peak in the unreacted fly ash spectra and therefore it was thought to be due to unreacted fly ash present in the AAB. The peak near 1000 cm^{-1} (most intense for raw fly ash powder at 1043 cm^{-1}) was indicative of silicate stretching and it shifted after the reactions which produced the AAB.

TABLE IV. CHARACTERISTIC SI-O-SI PEAK (SHIFT W.R.T. 1043 CM-1) FOR THE DIFFERENT AAB MIXTURES AT 28-DAY AGE

Mixture Proportion (AAB)	Characteristic Si-O-Si peak (Shift w.r.t. 1043 cm^{-1})		
	23˚C	40˚C	60˚C
FA 100	1018 (25)	1013 (30)	1003 (40)
FA 85 SG 15	1002 (41)	1000 (43)	998 (45)
FA 70 SG 30	998 (45)	996 (47)	993 (50)
FA 50 SG 50	984 (59)	980 (63)	975 (68)
FA 30 SG 70	962 (81)	956 (87)	959 (84)
FA 15 SG 85	949 (94)	946 (97)	942 (101)
FA 100 p15	1018 (25)	1013 (30)	1003 (40)
FA 100 p30	1018 (25)	1013 (30)	1003 (40)
FA 100 p60	1018 (25)	1013 (30)	1003 (40)

Following the reactions of the raw fly ash with the activating solution, a structural reorganization occurs in which aluminium ions are incorporated into the SiO_4 tetrahedra, forming the Si-O-Al network. The extent of the peak shift has been found previously to correlate with the amount of aluminium incorporated into the silicate structure at constant alkali content. Furthermore, the addition of alkali, forming non-bridging oxygens of the form $Si\text{-}O\text{-}Na^+$, causes a lowering of the molecular vibration force constant and therefore shifting of the peak associated with the asymmetric stretching of Si-O-Si(Al) bond to lower wavenumbers [31]. FTIR spectra were obtained for all the different mixture proportions at 28-day age. In Fig. 4 sample FTIR spectra for FA 100, FA 50 SG 50, and SG 100 samples cured at 40˚C temperature, are presented. Apart from the varied peak shift mentioned above, FTIR spectra for the AAB appeared quite similar, indicating that all have similar bonding on a molecular level. The peak shifts for the different AAB mixtures at 28-day age are shown in Table IV.

C. Scanning Electron Microscopy (SEM) and Energy Dispersive X-ray (EDS)

Figs. 5(a) through 5(f) show the typical microstructural features of FA 100 AAB samples at three different temperatures and two different magnifications at each temperature. In general, the microstructure of the FA 100 AAB samples was highly inhomogeneous and primarily made up of the reaction product resulting from the alkali activation – a sodium aluminosilicate gel that gave rise to the cementitious matrix. The matrix was full of loosely structured fly ash grains of different sizes. Numerous circular cavities belonging to fly ash particles were evident in the gel. Cavity surroundings consist of tubular vitreous network (Figs. 5(a) through (f)). Some small fly ash particles which have already reacted with the alkaline liquid, coexist with the unreacted particles (spherical vitreous particles of various sizes in the range of 10 – 200 μm). There were also some spherical particles partially covered with the reaction products (Fig. 5 (c) and (d)) which consequently reduced the rate of reactions to some extent.

FA 100 23 ℃

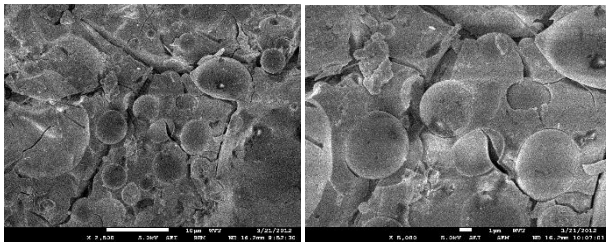

(a) 2500x (b) 5000x

FA 100 40 ℃

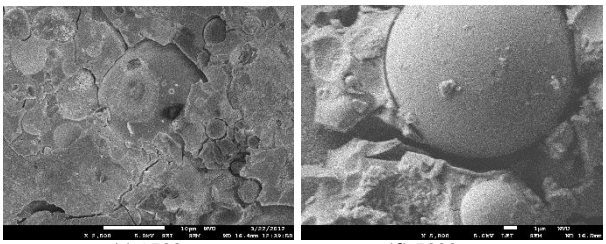

(c) 2500x (d) 5000x

FA 100 60 ℃

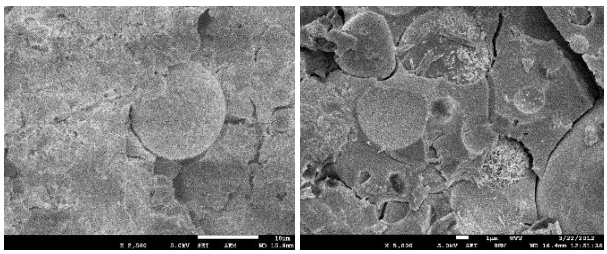

(e) 2500x (f) 5000x

Figure 5. Example SEM images of 28-days old FA 100 AAB samples at two different magnifications – 2500x and 5000x: (a) and (b) 23˚C, (c) and (d) 40˚C, and (e) and (f) 60˚C. Five different points were scanned at nine different locations on each sample at each magnification to obtain a total of 90 data points in each case.

FA 50 SG 50 40˚C

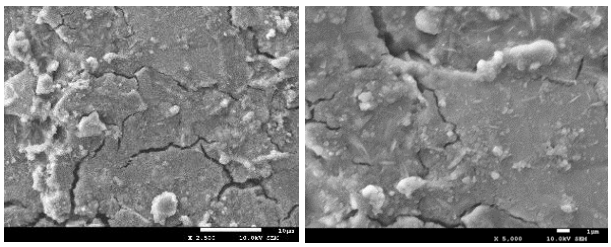

(a) 2500x (b) 5000x

SG 100 40˚C

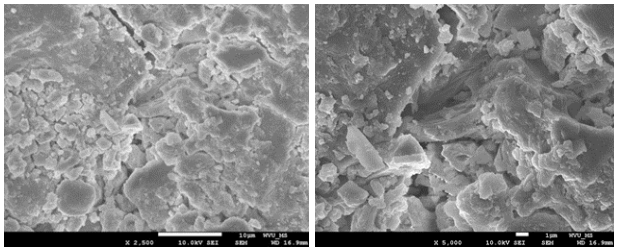

(c) 2500x (d) 5000x

Figure 6. Example SEM images of 28-days old AAB samples cured at 40˚C and at two different magnifications – 2500x and 5000x: (a) and (b) FA 50 SG 50, and (c) and (d) SG 100. Five different points were scanned at nine different locations on each sample at each magnification to obtain a total of 90 data points in each case.

The considerable amount of unreacted spheres, as well as the presence of pores in the matrix (Figs. 5 (a), 5 (c), 5 (d)) indicated incomplete reactions. The amount of sodium aluminosilicate gel present in the cementitious matrix was found to increase with the rise in curing temperature. Thus it corroborated the findings from the FTIR studies that the degree of reaction was enhanced at higher temperature. The unreacted spherical particles of FA 100 samples indicated incomplete reactions which confirmed the low degree of reaction values (about 28.9% after 28 days for a curing temperature of 40˚C). The patterns observed in the case of the present study are in agreement with the results obtained by [1], [11], [19], [29].

Figs. 6 (a) through (d) show the typical microstructural features of (i) FA 50 SG 50, and (ii) SG 100 AAB samples cured at 40˚C temperature and two different magnifications have been shown for each case.

The patterns observed in the case of the present study are in agreement with the results obtained by [29]. The lighter areas indicated the CSH(S) phase formed due to the hydration of slag. The CSH(S) was identified through SEM morphology from their fibrous to irregular grains forming reticular network. The preceding figures, thus, showed the co-existence of sodium aluminosilicate matrix due to alkali activation of fly ash and CSH(S) formation due to slag hydration. In the case of the preblended AAB samples, the SEM revealed morphologies similar to the normal AAB mixtures. The SEM observations were only good enough for qualitative characterization of the AAB microstructure by identification of the various chemical phases present there. As the present study required quantitative knowledge of the chemical phases present in the microstructure of the AAB samples, EDS analyses were conducted.

EDS analysis shows (Fig. 7) that the matrix primarily consisted of the phases containing Na-Si-Al in the bulk region in case of the samples where fly ash was the main precursor. In addition to Na, Si and Al, traces of Fe, Ca, K and Mg were also observed in these samples. These remnants (Fe, Ca, K, Mg) obviously represented the unreacted fly ash phases, which did not dissolve during alkali activation. When slag was present in greater amounts, the presence of Ca^{2+} was more prominent.

EDS microanalyses were carried out on a total of 90 data points for each sample as mentioned above. The results obtained from the microanalysis were in terms of the atomic percentages of the different elements present in the AAB binder microstructure. The Si/Al, Na/Al and and Ca/Si ratios were computed for each of the 90 data points. They were plotted on 3D axes using OriginPro 9 software as shown in Fig. 8. The concept of 3D plot was used to characterize the CSH and its phase compositions in the case of portland cement paste through the solution of simultaneous algebraic equations. The results of the works done by previous researchers showed that typical AAB composition proposed by [29] is generally expressed as $nM_2O\ Al_2O_3\ xSiO_2\ yH_2O$; where $1<n<1.6$; $2<x<3.5$; $3<y<7$; and M: Na, K [15].

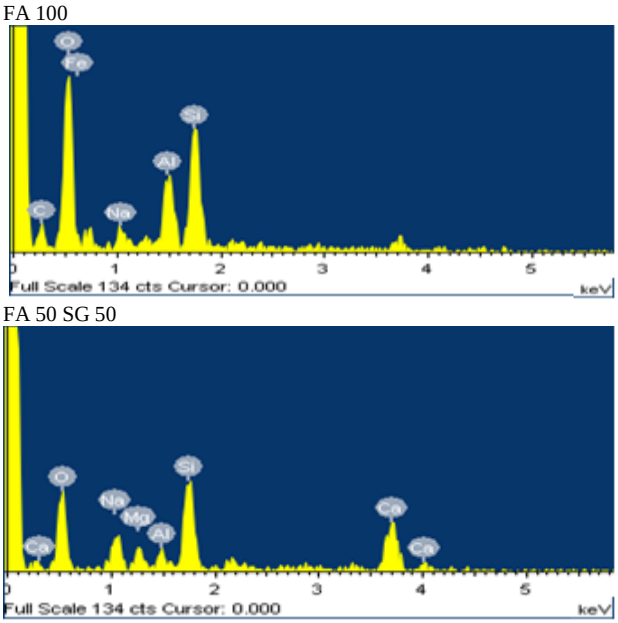

Figure 7. Example EDS images of 28-days old AAB samples cured at 40˚C: (a) FA 100 and (b) FA 50 SG 50. Five different points were scanned at nine different locations on each sample at each of two different magnifications to obtain a total of 90 data points in each case.

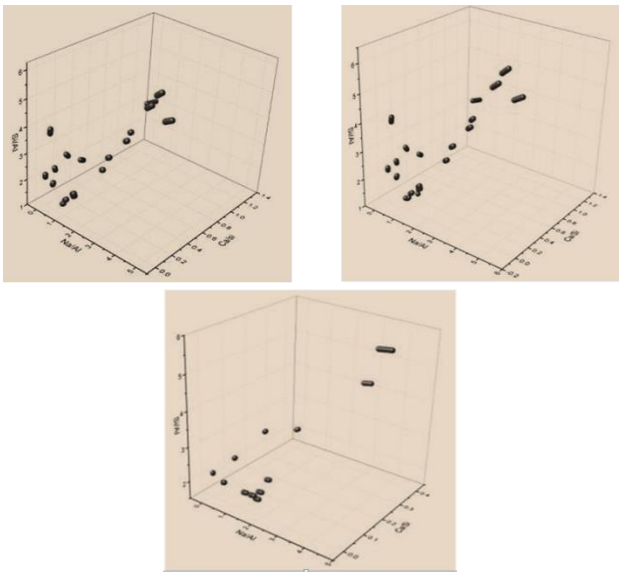

Figure 8. 3D plots of Na/Al, Si/Al and Ca/Si atomic ratios for a typical 7-day old FA 100 AAB at three different curing temperatures: 23˚C, 40˚C, and 60˚C.

The alkali activator in this study comprised of sodium silicate solution and sodium hydroxide. Hence, M represents Na, n represents the Na_2O/Al_2O_3 molar ratio, and x represents the SiO_2/Al_2O_3 molar ratio. From stoichiometry, it is evident that 1 mole of Na_2O is equivalent to 2 moles of Na; 1 mole of Al_2O_3 is equivalent to 2 moles of Al and 1 mole of SiO_2 is equivalent to 1 mole of Si. Hence the ranges for the oxide ratios mentioned above can be transformed to their equivalent elemental ratios as follows: 1<Na/Al (atomic ratio) <1.6 and 1<Si/Al< 1.75 (atomic ratio). These ranges will be used to analyze the results from the EDS analyses using the concept of 3-D plots. The total number

of points analyzed by EDS for each sample that comprised of Si/Al, and Na/Al ratios in the given range and Ca/Si ratios less than 0.1 were counted as representing the polymer product component of the total paste volume. It was assumed that the polymer products formed due to alkali activation of fly ash comprised of very low calcium content. Hence the Ca/Si ratios for these products were assumed to be less than 0.1. SEM-EDS microanalyses were carried out at randomly chosen points to account for the heterogeneity of the microstructure of the AAB. Each of the scanned areas was approximately 120 µm by 120 µm square. The polymer product was detected from SEM morphology and features, both at early stage and later. They were present as highly inhomogeneous structures and the matrix was full of loosely structured fly ash grains of different sizes. Numerous circular cavities belonging to fly ash particles were evident in the matrix. Cavities were surrounded by tubular vitreous network. The ratio of the number of points representing the polymer product to the total number of data points for each sample was taken as the representative volume fraction of polymer for each sample. This approach was somewhat similar to the point-count procedure as proposed by [33]. This approach had been successfully applied by the present authors for systems containing portland cement along with different combinations of fly ash, slag and silica fume as supplementary cementitious materials [34], [35]. The experimental volume fractions were compared with theoretical results as described in a previous study by the present authors [36]. The optimal Na/Al and Si/Al atomic ratios were obtained for each sample. Thus, unique values of *n*, *x* and *y* were obtained which most nearly represents the chemical composition of the polymer product. Similar approach was followed to find the volume fraction of CSH(S) in case of mixtures containing slag in addition to fly ash. The range of Ca/Si atom ratio in CSH(S) in case of slag cements is about 1.4 to 1.6 [35]. Thus, from the 3D plots of the microanalysis data, the number of points at which the Si/Ca ratio lies in the range of CSH(S) were counted and expressed as a fraction of the total number of data points. The volume fraction of the polymer product from the theoretical approach was computed using the *n*, *x*, and *y* values derived from the optimization technique. This was compared with the experimental values in case of the mixtures with slag and they showed very good agreement as furnished in a previous study by the present authors [35].

TABLE V. DEGREE OF REACTION OF ALKALI ACTIVATED FLY ASH AT DIFFERENT TEMPERATURES

Temperature	Age		
	7 days	28 days	90 days
23˚C	0.138	0.261	0.416
40˚C	0.147	0.270	0.475
60˚C	0.310	0.400	0.542

Three sample 3-D plots have been shown in Fig. 8. The 3-D plots of all mixtures are not furnished here for brevity. The first set of plots depicts the results at different curing temperatures for 7-day old FA 100 AAB samples. An increase in the number of points representing the reaction product due to alkali activation of fly ash was generally observed when the curing temperature was increased for both FA 100 mixtures as well as mixtures containing partial or full replacement of fly ash with slag.

D. Degree of Reaction

The degrees of reaction of alkali activated fly ash at different temperatures are presented in Table V. In order to validate the test results from the present study, the degree of fly ash reaction values were compared with the corresponding values from available literature. The comparisons are presented in Fig. 9. It was seen that the experimental values were in close agreement with the data from existing literature [32].

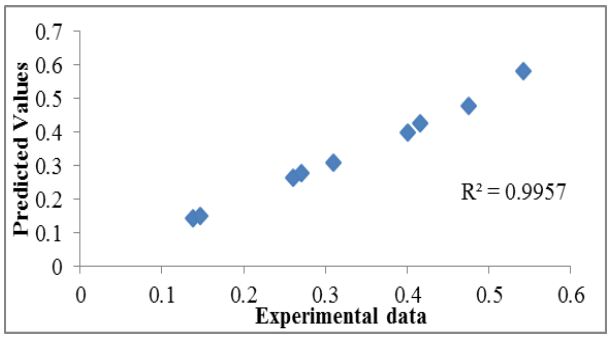

Figure 9. Correlation between values of degree of reaction of fly ash from present study and those from existing literature

TABLE VI. DEGREE OF REACTION OF ALKALI ACTIVATED SLAG AT DIFFERENT TEMPERATURES

Temp	Age		
	7 days	28 days	90 days
23˚C	0.25 (0.2 – 0.3)	0.35 (0.3 – 0.4)	0.55 (0.4 – 0.6)
40˚C	0.25 (0.2 – 0.3)	0.35 (0.3 – 0.4)	0.55 (0.4 – 0.6)
60˚C	0.25 (0.2 – 0.3)	0.35 (0.3 – 0.4)	0.55 (0.4 – 0.6)

In the case of degree of slag reaction, however, the values were obtained from a previous study by the present authors [35]. The study was conducted at constant temperature of 23˚C. From the findings of other researchers, it was observed that the degree of reaction of slag remained almost equal even at elevated temperatures [37]. The results of the slag degrees of hydration have been summarized in Table VI. The trend followed by the degree of reaction values directly influenced the volume fractions of the microstructural chemical components of the alkali-activated fly ash and slag, as presented in a previous study by the present authors [36].

E. Isothermal Calorimetry

The data obtained from the experiments are provided in the following plots of the heat flow from the AAB with respect to time. The plots of heat flow against time indicated the relative rates of hydration of the different AAB at different temperatures and different combinations

of precursors. For the sake of brevity, sample plots are provided in Fig. 10 to compare the isotherms for FA 100 AAB at different curing temperatures. Evidently, the heat evolved was the least for the sample cured at 23˚C, while it was the largest for the sample cured at 60˚C. The isotherms were practically identical for the normal FA 100 mixture and the FA 100 mixture preblended with NaOH for different durations at each temperature.

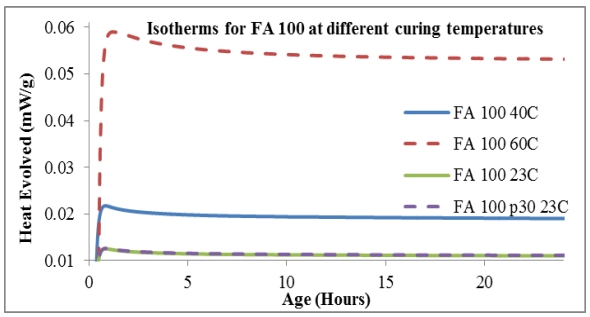

Figure 10. Isotherms for FA 100 at different curing temperatures.

The isotherm for FA 100 p30 has been shown as an example in Fig. 10. It was also observed that the area under the curve increased with increasing temperature. These results confirmed the findings from FTIR and SEM. Moreover, the trend of the degree of reaction values was confirmed by the nature of the isotherms. Isothermal calorimetry results showed that the area under the calorimetry curves for FA 100 AAB samples increased with increasing temperature which indicated higher degree of reaction at elevated curing temperatures.

V. Conclusions

XRD diffractograms showed the presence of mostly amorphous structure along with the presence of quartz, mullite, analcime, and hydroxyl sodalite peaks.

FTIR spectra showed the presence of Si-O-Si as well as Si-O-Al bonds and the presence of unreacted raw materials in microstructure of the AAB. The progress of reactions with increasing temperature or addition of Ca^{2+} ions through slag was also visible.

SEM images showed that in general, the microstructure of the FA 100 AAB samples was highly inhomogeneous and primarily made up of the reaction product resulting from the alkali activation – a sodium aluminosilicate gel that gave rise to the cementitious matrix. When slag was added, the lighter areas on the images indicated the CSH(S) phase formed due to the hydration of slag, identified through SEM morphology from their fibrous to irregular grains forming reticular network.

EDS analyses showed that the matrix primarily consisted of the phases containing Na-Si-Al in the bulk region in case of the samples where fly ash was the main precursor. In addition to Na, Si and Al, traces of Fe, Ca, K and Mg were also observed in these samples. These remnants (Fe, Ca, K, Mg) represented the unreacted fly ash during alkali activation. When slag was present in greater amounts, the presence of Ca^{2+} was more prominent.

The degree of reaction of fly ash based AAB was found to increase appreciably with increase in curing temperature. However, in case of slag based AAB, the degree of reaction remained more or less independent of curing temperature.

Isothermal calorimetry results showed that the area under the calorimetry curves for FA 100 AAB samples increased with increasing temperature which indicated higher degree of reaction at elevated curing temperatures.

VI. Scope for Future Work

A comprehensive data base can be formed for the chemical composition of the sodium aluminosilicate hydrate gel formed by the alkali-activation of fly ash by studying fly ash from different sources because they will have different oxide ratios.

SEM image analysis, mercury intrusion porosimetry, nitrogen absorption, or any other suitable techniques can be used to estimate the porosity and pore size distributions. This information can be used to study shrinkage behavior of concrete with AAB.

Quantitative X-Ray Diffraction (QXRD) and Magic Angle Spinning – Nuclear Magnetic Resonance (MAS – NMR) techniques can be used to validate or enhance the accuracy of the technique proposed in the present study to estimate the microstructural phase volume fractions.

XRD and FTIR techniques can be used to identify any possible influence of the HRWRA on the chemistry of AAB by the study of fly ash and/or slag blended with only the admixture and no alkali activator.

Acknowledgement

Special thanks are due to the American Society of Civil Engineers (ASCE) for providing the 2012 Freeman Fellowship to the first author in support of this research. The authors gratefully acknowledge Arrow concrete for donating fly ash and slag, and PQ Corporation for providing the sodium silicate solution used in this study. Special thanks to West Virginia Research Corporation for partial funding and Shared Research Facility of West Virginia University (WVU) for the SEM-EDS facility. The authors would also like to acknowledge the support of Dr. Ben Dawson-Andoh, (Professor, Wood Science and Technology, Division of Forestry and Natural Resources, WVU) for his help with the degree of reaction measurements of AAB.

References

[1] J. L. Provis and J. S. J. Van Deventer, *Geopolymers: Structure, Processing, Properties and Industrial Applications*, Woodhead: CRC Press, 2009.

[2] J. Davidovits, "Mineral polymers and methods of making them," US Patent 4349386, 1982.

[3] J. Davidovits, "Geopolymers: Inorganic polymeric new materials," *Journal of Materials Education*, vol. 16, pp. 91–139, 1994.

[4] C. Shi, P. Krivenko, and M. Roy, *Alkali-Activated Cements and Concretes*, Taylor & Francis, London and New York, 2006.

[5] J. Davidovits, "Geopolymers of the first generation: SILIFACE process," in *Proc. 1st International Conference on Geopolymer*, Compiegne, France, June 1–3, 1988, vol. 1, pp. 49-67.

[6] J. W. Smith and D. C. Comrie, "Geopolymeric building materials in third world countries," in *Proc. 1st International Conference on*

Geopolymer, Compiegne, France, June 1–3, 1988, vol. 1, pp. 89–92.
[7] J. Davidovits, "Geopolymers: Inorganic polymeric new materials," *Journal of Thermal Analysis*, vol. 37, pp. 1633–1656, 1991.
[8] J. G. S. Van Jaarsveld, "The physical and chemical characterisation of fly ash based geopolymers," Ph.D. dissertation, Department of Chemical Engineering, University of Melbourne, Melbourne, Australia, 2000.
[9] J. Davidovits, "Synthetic mineral polymer compound of the silicoaluminates family and preparation process," US Patent, 4472199, 1984.
[10] P. Kamhangrittirong, P. Suwanvitaya, P. Suwanvitaya, and P. Chindaprasirt, "Green binder technology development using fly ash based geopolymer," presented at the JSPS-DOST International Symposium on Environmental Engineering, Symposium on Harmonizing Infrastructure Development with the Environment, Phillipines, 2007.
[11] K. Kupwade-Patil and E. Allouche, "Effect of Alkali Silica Reaction (ASR) in geopolymer concrete," presented at the World of Coal Ash (WOCA) Conference, Devnver, CO, USA, May 9 - 12, 2011.
[12] K. Komnitsas and D. Zaharaki, "Geopolymerization: A review and prospects for the minerals industry," *Minerals Engineering*, vol. 20, pp. 1261–1277, 2007.
[13] C. Rees, G. C. Lukey, and J. S. J. Van Deventer, "The role of solid silicates on the formation of geopolymers derived from coal ash," presented at the International Symposium of Research Students on Material Science and Engineering, Department of Metallurgical and Materials Engineering, Indian Institute of Technology Madras, Chennai, India, December 20-22, 2004.
[14] D. W. Breck, *Zeolite Molecular Sieves, Structure, Chemistry and Use*, New York: John Wiley & Sons, 1974.
[15] V. F. F. Barbosa, K. J. D. Mackenzie, and C. Thaumaturgo, "Synthesis and thermal behaviour of potassium sialate geopolymers," *Materials Letters*, vol. 57, pp. 1477–1482, 2000.
[16] W. K. W. Lee and J. S. J. Van Deventer, "Effects of anions on the formation of aluminosilicate gel in geopolymers," *Industrial & Engineering Chemistry Research*, vol. 41, no. 18, pp. 4550–4558, 2002.
[17] E. M. Flaningen, H. Khatami, and H. A. Szymanski, "Moleculare sieve zeolite," in *Advan. Chem. Ser*, American Chemical Society, Washington D.C., 1971, vol. 101, p. 201.
[18] Davidovits, J., "Geopolymeric reactions in the economic future of cements and concretes: World-wide mitigation of carbon dioxide emission," in *Proc. 2nd International Conference on Geopolymer*, Saint Qunentin, France, June 30–July 2, 1999, pp. 111–121.
[19] M. N. Muzek, J. Zelic, and D. Jozic, "Microstructural Characteristics of geopolymers based on alkali-activated fly ash," *Chem. Biochem. Eng. Q*., vol. 26, no. 2, pp. 89–95, 2012.
[20] P. D. Silva, K. Sagoe-Crenstil, and V. Sirivivatnanon, "Kinetics of geopolymerization: Role of Al_2O_3 and SiO_2," *Cem., Concr. Res.*, vol. 37, pp. 512–518, 2007.
[21] R. R. Lloyd, J. L. Provis, and J. S. J. Van Deventer, "Microscopy and microanalysis of inorganic polymer cements. 2: The gel binder," *J. Mater. Sci*., vol. 44, no. 2, pp. 620–631, 2009.
[22] Standard Specification for Coal Fly Ash and Raw or Calcined Natural Pozzolan for Use in Concrete, Annual Book of ASTM Standards. 04.02, Concrete and Aggregates, American Society for Testing and Materials, ASTM C618, 2013.
[23] Standard Specification for Slag Cement for Use in Concrete and Mortars, Annual Book of ASTM Standards. 04.02, Concrete and Aggregates, American Society for Testing and Materials. ASTM C989–2013.
[24] Standard Specification for Concrete Aggregates), Annual Book of ASTM Standards. 04.02, Concrete and Aggregates, American Society for Testing and Materials, ASTM C33/C33M–2013.
[25] Specification for Chemical Admixtures for Concrete, Annual Book of ASTM Standards. 04.02, Concrete and Aggregates, American Society for Testing and Materials. ASTM C494 Type F, 2013.
[26] A. Kar, U. B. Halabe, I. Ray, and A. Unnikrishnan, "Nondestructive characterizations of alkali activated fly ash and/or slag concrete," *European Scientific Journal*, vol. 9, no. 24, pp. 52–74, 2013.
[27] A. Fernandez-Jimenez, A. G. D. L. Torre, A. Palomo, G. Lopez-Olmo, M. M. Alonso, and M. A. G. Aranda, "Quantitative determination of phases in the alkaline activation of fly ash. Part II: Degree of reaction," *Fuel*, vol. 85, pp. 1960–1969, 2006.
[28] Standard Practice for Measuring Hydration Kinetics of Hydraulic Cementitious Mixtures Using Isothermal Calorimetry, Annual Book of ASTM Standards. 04.02, Concrete and Aggregates, American Society for Testing and Materials, ASTM C1679-09, 2013.
[29] F. Skvara, L. Kopecky, J. Nemecek, and Z. Bittnar, "Microstructure of geopolymer materials based on fly ash," *Cermaics–Silikaty*, vol. 50, pp. 208–215, 2006.
[30] A. R. Sakulich, "Characterization of environmentally-friendly alkali activated slag cements and ancient building materials," Ph.D. dissertation, Drexel University, Philadelphia, PA, USA, September 2009.
[31] C. A. Rees, "Mechanisms and kinetics of gel formation in geopolymers," Ph.D. dissertation, Department of Chemical and Biomolecular Engineering, University of Melbourne, Melbourne, Australia, March 2007.
[32] V. Smilauer, P. Hlavacek, F. Skvara, R. Sulc, L. Kopecky, and J. Nemecek, "Micromechanical multiscale model for alkali activation of fly ash and metakaolin," *J. Mater. Sci.*, 2011.
[33] X. Feng, E. J. Garboczi, D. P. Bentz, P. E. Stutzman, and T. O. Mason, "Estimation of the degree of hydration of blended cement pastes by a scanning electron microscopy point-count procedure," *Cement and Concrete Research*, vol. 34, no. 10, pp. 1787–1793, 2004.
[34] A. Kar, I. Ray, A. Unnikrishnan, and J. F. Davalos, "Microanalysis and optimization-based estimation of C-S-H contents of cementitious systems containing fly ash and silica fume," *Cement & Concrete Composites*, vol. 34, pp. 419–429, 2012.
[35] A. Kar, I. Ray, A. Unnikrishnan, and J. F. Davalos, "Estimation of C-S-H and calcium hydroxide for cement pastes containing slag and silica fume," *Construction and Building Materials*, vol. 30, pp. 505–515, 2012.
[36] A. Kar, I. Ray, U. B. Halabe, A. Unnikrishnan, and B. Dawson-Andoh, "Characterizations and estimation of alkali activated binder paste from microstructures," *International Journal of Concrete Structures and Materials*, vol. 8, no. 3, pp. 213-228, 2014.
[37] A. Fernandez-Jimenez and F. Puertas, "Alkali-Activated slag cements: Kinetic studies," *Cement and Concrete Research*, vol. 27, no. 3, pp. 359–368, 1997.

Arkamitra Kar is an Assistant Professor in Civil Engineering at BITS-Pilani, Hyderabad Campus. He received his M.S. (2008) and Ph.D. (2013) in Civil Engineering from West Virginia University (WVU) in USA. His research interests include characterization of binder systems at microstructural and specimen levels. He received the BITS Outstanding Potential for Excellence in Research and Academics (OPERA) award in 2015, the 2013 WVU Dissertation Fellowship, and 2012 ASCE Freeman Fellowship.

Indrajit Ray is Ph.D. in civil engineering. He is working as the Professor and Program Coordinator of Construction Engineering, Materials, and Management at the Department of Civil and Environmental Engineering, Faculty of Engineering, The University of the West Indies, St Augustine, Trinidad and Tobago. He has over 25 years of experience in research on characterization of cementitious systems; properties of green and sustainable construction materials; FRP-concrete composites. He published several peer-reviewed articles and advised scores of graduate students.

Udaya B. Halabe is a Professor of Civil and Environmental Engineering at West Virginia University, Morgantown, WV. He received M.S. and Ph.D. degrees in Civil/Structural Engineering from the Massachusetts Institute of Technology (MIT) in 1988 and 1990, respectively. He is a Fellow of ASCE, SEI, ASNT, and member of ACI and ASEE.

Avinash Unnkirishnan is an Associate Professor, Civil and Environmental Engineering at Portland State University, Oregon. He received his Ph.D. from University of Texas, Austin. His research focus is Transportation Engineering and application of statistical techniques to civil infrastructure systems.